Uniosun Journal of Engineering and Environmental Sciences (UJEES), Vol. 8 No. 2, Sept., 2026
DOI: 10.64980/ujees.v8i2.003 **Abdulazeez et al.**
Published: September 30, 2026

MINIMIZING THE OUTAGE PERFORMANCE OF UAV-BASED COOPERATIVE NOMA NETWORK WITH HYBRID TIME POWER SPLITTING SCHEME UNDER OPTIMAL SYSTEM PARAMETERS

Fausat I. ABDULAZEEZ[1], Damilare O. AKANDE[2*], and Samson I. OJO[3]

[1,2,3]*Electronic and Electrical Engineering Department, Ladoke Akintola University of Technology, Ogbomoso, Nigeria*

[*]*Corresponding Author: doakande@lautech.edu.ng*

Abstract
Driven by the need for more energy-efficient and high-capacity wireless systems, studies are increasingly focusing on NOMA-based cooperative UAV networks that utilize the Hybrid Time Power Splitting (HTPS) scheme. Though, to ensure efficient and reliable system performance, optimization is required to minimize the UAV's energy consumption by finding the best combination of hovering time, trajectory and resource allocation but the performance depends on system parameters. Hence, in this paper, we analyzed the performance of Hybrid Time Power Splitting optimized with Enhanced Duck Swarm Algorithm (HTPS -EDSA) using Roulette Wheel Selection (RWS) under varying system parameters. A closed form outage probability analysis of the HTPS scheme for UAV-aided cooperative NOMA network over Nakagami-m fading channel was derived. An outage probability optimization problem with consideration for the resource constraints to improve the reliability of the network was formulated. The formulated problem was solved using EDSA. The HTPS -EDSA scheme was simulated using MATLAB R2023a, and the performance analysis was carried out using outage probability under varying system parameters, including transmit power, UAV altitude, fraction of received power, and energy harvesting time. The result obtained showed that the outage probability improved at optimal values of the UAV altitude, fractions of the energy harvesting time and received power. Also, a distinct optimal power-splitting ratio was found at 0.7, minimizing outage probability to approximately 5.27 x 10^{-8} as compared to conventional HTPS, HTPS with Duck Swarm Algorithm (HTPS-DSA) and HTPS with Bat Algorithm Optimization (HTPS-BAO) which gave 3.527 x 10^{-8}, 7.65 x 10^{-8} and 1.12 x 10^{-8}, respectively.

Keywords
Full-duplex relaying, Nakagami-m fading, Roulette Wheel Selection, Bio-inspired optimization, Energy harvesting

1. INTRODUCTION

Unmanned Aerial Vehicles (UAVs) offer a revolutionary approach to enhancing wireless network connectivity by dynamically adjusting their altitude and maneuvering around difficult and physical obstructions such as buildings and terrain, making them ideal for establishing reliable Line of Sight (LoS) links with end-users. However, their battery-powered nature limits operational duration. To address this, researchers have developed Simultaneous Wireless Information and Power Transfer (SWIPT), which enables UAVs to harvest energy and receive data from a single wireless signal, thereby extending deployment time without manual and frequent [1],[2]. SWIPT typically employs two main schemes: Time Switching (TS) and Power Splitting (PS) [3], [4]. TS alternates between energy harvesting and information decoding over time, while PS divides the received signal into two concurrent streams, one for energy harvesting and the other for information decoding. Although both TS and PS have drawn significant research interest, their effectiveness is highly sensitive to channel conditions. Time Splitting (TS) tends to outperform PS under low SNR, whereas PS becomes more favorable in high SNR scenarios [5],[6]. To exploit the advantages of both, the Hybrid Time-Power Splitting (HTPS) scheme has been proposed, which enhances energy harvesting efficiency and system performance relative to conventional approaches [7],[8].

Moreover, UAVs often operate in spectrum-constrained environments such as urban centers or disaster-stricken regions, requiring Non-Orthogonal Multiple Access (NOMA) to maximize spectral efficiency. By enabling simultaneous access to the same resource block, NOMA reduces latency compared to Orthogonal Multiple Access (OMA) [9],[10]. NOMA offers flexibility for dynamic UAV networks by reducing resource allocation overhead [11],[12] and provides spectral efficiency and massive connectivity [13], yet its performance is constrained by interference, mobility and energy limitations [14],[15]. Cooperative Non-Orthogonal Multiple Access (CNOMA) overcomes these challenges through user cooperation, enabling more

robust and reliable UAV communications. As a result, CNOMA enhances spectrum utilization, connectivity, and system performance, making it highly beneficial for UAV-aided wireless networks [5].

The growing demand for energy-efficient, high-capacity wireless communication has spurred extensive research into multiple access schemes for UAV networks capable of integrating SWIPT technologies. NOMA has gained traction for its spectral efficiency and resource allocation benefits; however, its performance is hindered by inter-user interference, reliance on effective Successive Interference Cancellation (SIC) implementation, and degradation when users have similar channel gains [16]. These challenges are further exacerbated in fast-varying, energy-constrained environments. From an energy harvesting standpoint, time splitting suffers from low spectral efficiency and latency due to its sequential operation, while power splitting compromises signal quality under rapidly changing UAV conditions [5]. Moreover, optimizing UAV-aided NOMA networks is complicated by UAV mobility, diverse user requirements, and frequent channel fluctuations [17].

Existing literature has sought to mitigate challenges in UAV-NOMA networks through various approaches. Vo et al. [5] applied a hybrid TPS-SWIPT scheme with joint parameter optimization to minimize outages, though their Bat Algorithm Optimization (BAO) exhibited premature convergence and local optima issues. The author in [18] explored resource allocation in full-duplex UAV-NOMA with SWIPT to boost weak user rates but relied on idealistic assumptions including perfect self-interference cancellation, simplified SIC, and lossless energy conversion, overlooking mobility and energy dissipation. Sadeeq and Ahmed [19] introduced a hybrid OMA-NOMA framework for UAV-BS networks with multiple antennas to balance throughput and fairness yet assumed perfect CSI and disregarded UAV energy constraints.

In practice, UAVs operate under severe energy limitations, real-world mobility, and dynamic environmental changes, all of which result in imperfect Channel State Information (CSI). Nonetheless, this analysis adopts perfect CSI, derived from the channel gain, to enable tractable outage probability analysis. Consequently, despite notable progress, SWIPT-aided UAV-NOMA networks remain constrained by oversimplified channel and energy models, while algorithms like the conventional Duck Swarm Algorithm (DSA) [20] and BAO suffer from premature convergence deficiencies which makes them to be easily trapped in local minima. Critically, the joint optimization of HTPS schemes with UAV trajectory under realistic fading conditions remains largely unexplored. This highlights a critical need for enhanced bio-inspired metaheuristics optimization method on outage performance and analyze its effect on system parameters. Table 1 presents a summary of the related literature in this area of study. This paper closes these gaps by formulating a joint outage probability minimization problem based on instantaneous network resources. The solution to the formulated problem carried out using DSA enhanced with RWS optimizer. The core contributions of this paper are summarized as follows:

1) We examine the effects of key system parameters, including energy harvesting duration, power-splitting ratios, and UAV altitude, on the outage probability of the FD UAV-based CNOMA network over Nakagami-m fading channel.
2) We establish optimal operating conditions for key design parameters, providing an insights for future energy-efficient UAV-aided wireless networks. This is achieved through DSA with Roulette Wheel Selection (RWS), which mitigates the random leader update limitation of conventional DSA via greedy selection .

Table 1: Summary of related literature

Study	Optimization Algorithm	UAV Model	SWIPT Scheme	Objective	Limitation
[5]	Bat Algorithm	Fixed altitude, Half duplex	Hybrid TS/PS	Minimize outage probability	Premature convergence, local optima
[7]	None stated	MEC-assisted UAV	SWIPT	Maximize energy charging	No cooperative NOMA / outage analysis
[18]	None (analytical)	Full duplex, fixed	SWIPT (single scheme)	Boost weak-user rate	Fixed energy harvesting ratio
[19]	None (analytical)	Multi-antenna BS, fixed	OMA-NOMA hybrid	Balance throughput & fairness	Perfect CSI; no UAV energy constraint
This work	DSA enhanced with RWS	Optimal altitude, power	HTPS with joint optimal ρ, τ	Minimize outage probability	

allocation,
perfect CSI

2. MATERIALS AND METHOD

2.1. System Model

Fig. 1 depicts a downlink cooperative NOMA system where direct communication between devices is blocked due to severe fading. A UAV relay (UAVR) harvests energy from the source signal and forwards the decoded data to the destinations. The source, UAV relay and destination channels are quasi-static and undergo independent, non-identically distributed Nakagami-m fading ensuring a LoS dominance with perfect CSI assumed at the UAVR for the purpose of deriving a closed-form outage performance. The UAVR hovers at an optimal altitude and location for the duration of a transmission block. In addition, the UAVR operates in full-duplex mode, which causes self-interference because of concurrent transmission between its transmit and receiving antennas. To mitigate the interference, perfect successive interference cancellation is assumed. A block frame of the HTPS scheme as detailed in Fig. 2 with a total transmission duration of T is partitioned into three distinct phases is assumed static during the transmission to the destinations. During the first phase, denoted as τT, UAVR harvests energy from the source, where $0 < \tau < 1$ denotes the fraction of block time for EH in the downlink scenario. During the second phase, denoted as $(1-\tau)\,T/2$, the UAVR employs a portion ρ of the received power for EH, while the remaining fraction $(1-\rho)$ is allocated for information decoding as ρ represents the power splitting ratio, which satisfies the condition $0 < \rho < 1$. During the third phase, denoted as $(1-\tau)\,T/2$, the UAVR employs the energy it has harvested to transmit the received signal to the destination. The UAVR superimposed its information with the decoded signal and sent it to near user and far user. The near user is for the source's destination while the far user is for the relay's destination. Based on this time frame, the downlink scenario of the system considered is employed in three phases, namely the EH phase and direct information transmission phase (First phase), information decoding phase (Second phase), and the relaying transmission phase (Third phase).

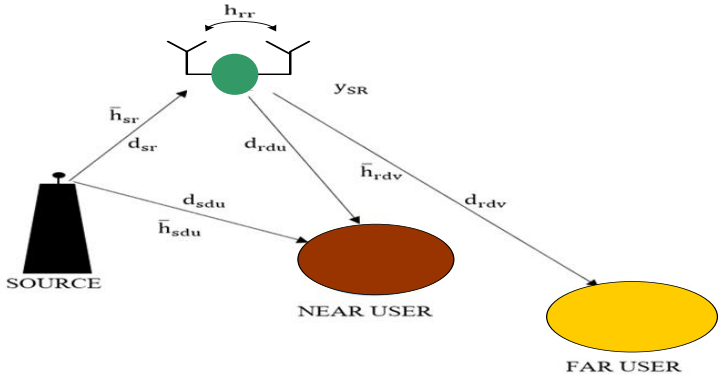


Fig.1: System model

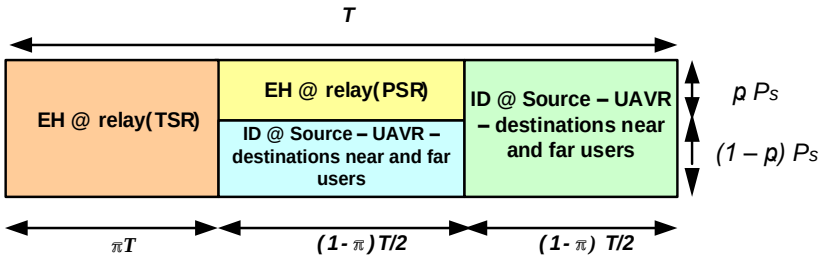


Fig.2: Framework, a total transmission block of duration

The received signal at UAVR in the first phase can be expressed according to Ding *et al.*, (2016) as

$$y_{SR} = \left(\sqrt{\frac{\alpha_{U_{i^*}} P_S}{d_{SA}^{\theta_{SA}}}} x_{U_{i^*}} + \sqrt{\frac{\alpha_{V_{j^*}} P_S}{d_{SA}^{\theta_{SA}}}} x_{V_{j^*}} \right) h_{SA} + h_{rr} + n_{SA} \qquad (1)$$

where $\alpha_{U_i} + \alpha_{V_j} = 1,\ \alpha_{U_i}$and $\alpha_{V_j} > 0.$ $\alpha_{U_i}$and α_{V_j} are the power allocation coefficients of the destination U_i and V_j at the source respectively, P_S is the source transmit power, x_{U_i} and x_{V_j} is a transmit signals, h_{SA} is the channel coefficient between the source and UAVR and modelled as a complex fading coefficient whose envelope $|h_{SA}|$ follows a Nakagami-m distribution with parameter Ω_{SA} (average fading power) and shape $m_{SA} = 0.5$, h_{rr} is the residual channel coefficient (self interference of UAVR), modelled its amplitude $|h_{rr}|$ with Nakagami parameters m_{rr}, Ω_{rr}. n_{SA} is the Additive White Gaussian Noise, d_{SA} is the distance between the source and UAVR and θ_{SA} is the path loss exponent for the source and UAVR.

The UAVR exhibit self-interference, therefore the signal-to-interference-plus-noise ratio (SINRs) for decoding the received signal at U_i and V_j are obtained as

$$\gamma_{SU}^{x_{U_{i^*}}} = \frac{\alpha_{U_{i^*}}\ \gamma_0\ |\hat{h}_{SU_{i^*}}|^2}{\alpha_{V_{j^*}}\gamma_0|\hat{h}_{SU_{i^*}}|^2\ |\hat{h}_{rr}|^2\ + \gamma_0\ \sigma^2_{SU_{i^*}}\ |\hat{h}_{rr}|^2\ +\ 1} \tag{2}$$

$$\gamma_{SV_{j^*}}^{x_{U_{i^*}}} = \frac{\alpha_{U_{i^*}}\ \gamma_0\ |\ \hat{h}_{SV_{j^*}}|^2}{\alpha_{V_{j^*}}\ \gamma_0\ |\hat{h}_{SV_{j^*}}|^2\ \ |\hat{h}_{rr}\ |^2\ +\ \gamma_0\ \sigma^2_{SV_{j^*}}\ |\hat{h}_{rr}|^2\ +\ 1} \tag{3}$$

$$\gamma_{SV_{j^*}}^{xV_{j^*}} = \frac{\alpha_{V_{j^*}}\ \gamma_0\ |\hat{h}_{SV_{j^*}}|^2}{\gamma_0\ \sigma^2_{SV_{j^*}}\ |\hat{h}_{rr}|^2\ +\ 1} \tag{4}$$

where $\gamma_0 = P_S/N_0$. Similarly, the received signal at the kth antenna of the UAVR R_k is expressed as

$$y_{SR_k} = \left(\sqrt{\frac{\alpha_{U_{i^*}}P}{d^{\theta}_{SR_k}}}x_{U_{i^*}}\ +\ \sqrt{\frac{\alpha_{V_{j^*}}P_S}{d^{\theta}_{SR_k}}}x_{V_{j^*}}\right)h_{SR_k}\ +\ h_{rr}\ +\ n_{SR_k} \tag{5}$$

where $n_{SR_k} \sim CN(0, N_o)$.

The EH of the kth antenna of the UAVR in the first phase using TS scheme is obtained as

$$E_{R_k}^{(TS)}\ =\ \eta\tau TP_S|\hat{h}_{SR_k}|^2 =\ \eta\tau TP_S\frac{\left|\bar{h}_{SR_k}\right|^2}{d^{\theta}_{SR_k}} \tag{6}$$

In the second phase, for information decoding, the received signal at kth antenna of the UAVR becomes:

$$y_{SR_k} = \sqrt{1\ -\ \rho}\left(\sqrt{\frac{\alpha_{U_{i^*}}P_S}{d^{\theta}_{SR_k}}}x_{U_{i^*}} + \sqrt{\frac{\alpha_{V_{j^*}}P_S}{d^{\theta}_{SR_k}}}\ x_{V_{j^*}}\right)h_{SR_k}\ +\ h_{rr} + n_{SR_k} \tag{7}$$

Therefore, the EH during the second phase using PS scheme can be written as

$$E_{R_k}^{(PS)}\ =\ \frac{\eta\rho(1-\tau)TP_S\,|\hat{h}_{SR_k}|^2}{2} \tag{8}$$

The SINRs for decoding $x_{U_{i^*}}$and $x_{V_{j^*}}$ can be written respectively as:

$$\gamma_{SR_k}^{x_{U_{i^*}}} = \frac{(1-\rho\ )\alpha_{U_{i^*}}\ \gamma_0\ |\hat{h}_{SR_k}|^2}{(1-\rho)\ \alpha_{V_{j^*}}\ \gamma_0\ |\hat{h}_{SR_k}|^2|h_{rr}|^2 + (1-\rho)\gamma_0\ \sigma^2_{SR_k}\ |h_{rr}|^2 + 1} \tag{9}$$

$$\gamma_{SR_k}^{x_{V_{j^*}}} = \frac{(1-\rho)\alpha_{v_{j^*}}\ \gamma_0\ |\hat{h}_{SR_k}|^2}{(1-\rho)\ \gamma_0\sigma^2_{SR_k}\ |h_{rr}|^2\ +1} \tag{10}$$

In the third phase, i.e the relaying transmission phase, the energy harvested is utilized as transmit power for the relaying transmission. Specifically, using the HTPS scheme, the total amount of energy harvested at the kth antenna of the UAVR is obtained by summing equations (3.6) and (3.8) and is obtained as

$$E_{R_k}^{HTPS} = E_{R_k}^{TS}\ +\ E_{R_k}^{PS} =\ \eta TP_S\left(\tau|\hat{h}_{SR_k}|^2 + \frac{\rho(1-\tau)|\hat{h}_{SR_k}|^2}{2}\right) \tag{11}$$

Thus, the received signal in the third phase is written as:

$$y_{R_{k^A}} = \left(\sqrt{\frac{\beta_{U_{i^*}}P_{R_k}}{d^{\theta}_{R_k,A}}}x_{U_{i^*}}\ +\ \sqrt{\frac{\beta_{V_{j^*}}P_{R_k}}{d^{\theta}_{R_k,A}}}x_{V_{j^*}}\right)h_{R_{k^A}}\ +\ h_{rr}\ +\ n_{R_{k^A}} \tag{12}$$

where $n_{R_{k^A}} \sim CN\ (0, N_o)$; $\beta_{U_{i^*}}$ and $\beta_{V_{j^*}}$ are the power allocation coefficients of the destination. U_i and V_j and at the UAVR, respectively and $\beta_{U_i}\ +\ \beta_{V_j} = 1$ and $\beta_{U_i}\ and\ \beta_{V_j} > 0.$

In the second phase, UAVR forwards information during a transmission interval of $\frac{(1-\tau)T}{2}$, thus the transmit power from UAVR at the kth antenna in the transmission phase with the HTPS is obtained by dividing equation (11) by the transmission time T, and expressed as

$$P_{R_k} = \frac{E_{R_k}^{HTPS}}{(1-\tau)T/2} = \eta P_S \left|\hat{h}_{SR_k}\right|^2 \left(\frac{2\tau}{(1-\tau)} + \rho\right) \quad (13)$$

Considering the UAVR self-interference, the effective transmitting power in the transmission phase with HTPS is expressed as

$$P_{R_k} = \frac{E_{R_k}^{HTPS}}{(1-\tau)T/2} = \eta P_S |\hat{h}_{SR_k}|^2 |h_{rr}|^2 \left(\frac{2\tau}{(1-\tau)} + \rho\right). \quad (14)$$

Therefore, the SINRs obtained from the received signal in equation (12) for the near user U_{i^*} and far user V_{j^*} after decoding $x_{U_{i^*}}$ and $x_{V_{j^*}}$ at the UAVR are expressed as

$$\gamma_{R_k U_{i^*}}^{x_{U_{i^*}}} = \frac{\beta_{U_{i^*}} \gamma_{R_k} |\hat{h}_{R_k U_{i^*}}|^2}{\beta_{V_{j^*}} \gamma_{R_k} |\hat{h}_{R_k U_{i^*}}|^2 |h_{R_k R_k}|^2 + \gamma_{R_k} \sigma^2_{R_k U_{i^*}} |h_{R_k R_k}|^2 + 1} \quad (16)$$

$$\gamma_{R_k V_{j^*}}^{x_{U_{i^*}}} = \frac{\beta_{U_{i^*}} \gamma_{R_k} |\hat{h}_{R_k V_{j^*}}|^2}{\beta_{V_{j^*}} \gamma_{R_k} |\hat{h}_{R_k V_{j^*}}|^2 |h_{R_k R_k}|^2 + \gamma_{R_k} \sigma^2_{R_k V_{j^*}} + 1} \quad (17)$$

$$\gamma_{R_k V_{j^*}}^{x_{V_{j^*}}} = \frac{\beta_{V_{j^*}} \gamma_{R_k} |\hat{h}_{R_k V_{j^*}}|^2}{\gamma_{R_k} \sigma^2_{R_k V_{j^*}} + 1} \quad (18)$$

where $|\hat{h}_{R_k A}|^2 = |\bar{h}_{R_k A}|^2 / d_{R_k,A}^{\theta}$, $\gamma_{R_k} = P_{R_k}/N_0$ and $A \in \{U_{i^*}, V_{j^*}\}$. Furthermore, the end-to-end SINR of the system considered can be expressed as:

$$\gamma_{e2e}^{SR_k UV} = min\left\{\gamma_{SR_k}, \gamma_{SR_k}^{x_{U_{i^*}}}, \gamma_{SR_k}^{x_{V_{j^*}}}, \gamma_{R_k U_{i^*}}^{x_{U_{i^*}}}, \gamma_{R_k V_{j^*}}^{x_{U_{i^*}}}, \gamma_{R_k V_{j^*}}^{x_{V_{j^*}}}\right\} \quad (19)$$

The optimal selected kth antenna of the UAVR is chosen such that the end-to-end SINR is maximum to improve the outage probability performance and is can be written as

$$\gamma_{e2e}^{(d)} = \max_{1 \le k \le k} \left\{\gamma_{e2e}^{SR_k UV}\right\} \quad (20)$$

2.2 Outage Probability Analysis

In the optimized HTPS scheme, the interruption in communication transmission occurs when both the direct SINR and the end-to-end SINR at the destination drop below a predefined outage threshold. Consequently, the outage probability (P_{out}) for the proposed scheme is expressed according to Zhang et al. [21]as

$$P_{out} = \mathrm{P_r}\{\gamma_{e2e}^{SR_k UV} < \gamma^{(d)}\} \quad (21)$$

Equation (21) can simply be rewritten sa

$$P_{out} = P^U + P^V - P^{UV} = P^{SR_k UV}(P^{SU} + P^{SV} - P^{SU} P^{SV}) \quad (22)$$

where

$$P^{SU} = Pr\left\{\gamma_{SU_{j^*}}^{x_{U_{i^*}}} < \gamma^{(d)}\right\} \quad (23)$$

$$P^{SV} = Pr\left\{\gamma_{SV_{j^*}}^{x_{U_{i^*}}} < \gamma^{(d)}, \gamma_{SV_{j^*}}^{x_{V_{j^*}}} < \gamma^{(d)}\right\} \quad (24)$$

$$P^{SR_k UV} = Pr\left\{\gamma_{e2e}^{(d)} < \gamma^{(d)}\right\} \quad (25)$$

where $\gamma^{(d)} = 2^{2R} - 1$ is the threshold SNR.

Therefore, by substituting equation (2) into equation (23), the probability is obtained as

$$P^{SU} = Pr\left\{\frac{\alpha_{U_{i^*}} \gamma_0 |\hat{h}_{SU_{i^*}}|^2}{\alpha_{V_{j^*}} \gamma_0 |\hat{h}_{SU_{i^*}}|^2 + \gamma_0 \sigma^2_{SU_{i^*}} + 1} < \gamma^{(d)}\right\} \quad (26)$$

By isolating $|\hat{h}_{SU_{i^*}}|^2$, equation (26) is reformulated as

$$P^{SU} = Pr\left\{|\hat{h}_{SU_{i^*}}|^2 < \frac{\gamma^{(d)}\left(\gamma_0 \sigma^2_{SU_{i^*}} + 1\right)}{\gamma_0\left(\alpha_{U_{i^*}} - \gamma^{(d)} \alpha_{V_{j^*}}\right)}\right\} \quad (27)$$

For Nakagami-m fading channel experienced in equation (27), the instantaneous channel gain $\hat{\mathrm{h}}_{\mathrm{SU_{i^*}}}|^2$ follows a Gamma distribution with its Probability Density Function (PDF) expressed as [22]

$$f\left(|\hat{h}_{SU_{i^*}}|^2\right) = \left(\frac{m}{\lambda}\right)^m \frac{\left[|\hat{h}_{SU_{i^*}}|^2\right]^{m-1}}{\Gamma(m)} exp\left(-\frac{m}{\lambda}|\hat{h}_{SU_{i^*}}|^2\right) \quad (28)$$

where $m = m_{SU_{i^*}} = \mathrm{m}_{\mathrm{SV}_{j^*}} = 0.5$ for simplicity and is the Nakagami fading severity parameter characterized with dominance LoS, $\lambda = \mathbb{E}\left[|\hat{h}_{SU_{i^*}}|^2\right]$ is the average channel power and $\Gamma(m)$ is the gamma function (for integer m, $\Gamma(m) = (m-1)!$). By applying the Cumulative Distribution Function (CDF) of the gamma distribution of the outage probability in equation (27) is given as

$$P^{SU} = Pr\left\{|\hat{h}_{SU_{i^*}}|^2 < \mathcal{T}\right\} = \int_0^{\mathcal{T}} \left(\frac{m}{\lambda}\right)^m \frac{\left[|\hat{h}_{SU_{i^*}}|^2\right]^{m-1}}{\Gamma(m)} exp\left(-\frac{m}{\lambda}|\hat{h}_{SU_{i^*}}|^2\right) d|\hat{h}_{SU_{i^*}}|^2 \quad (29)$$

where $\mathcal{T} = \frac{\kappa_1 \gamma^{(d)}}{\gamma_0\left(\alpha_U - \alpha_V \gamma^{(d)}\right)}$.

Equation (29) can be solved by applying the lower incomplete gamma function [22]

$$\int_0^{\mathcal{T}} \left[|\hat{h}_{SU_{i^*}}|^2\right]^{m-1} exp\left(-\frac{m}{\lambda}|\hat{h}_{SU_{i^*}}|^2\right) d|\hat{h}_{SU_{i^*}}|^2 = \left(\frac{m}{\lambda}\right)^{-m} \gamma\left(m, \frac{m}{\lambda}\mathcal{T}\right) \quad (30)$$

where $\gamma(m, x) = \Gamma(m)\left[1 - exp\left(-\frac{m}{\lambda}\mathcal{T}\right)\sum_{p=0}^{m-1}\frac{\left(\frac{m}{\lambda}\mathcal{T}\right)^p}{p!}\right]$ is the lower incomplete gamma function with a closed-form series. The outage probability which is the CDF of the channel gain $|\hat{h}_{SU_{i^*}}|^2$ is then obtained by simplifying equation (30) and substituting into equations (29) as

$$P^{SU} = 1 - \sum_{p=0}^{m_{SU_{i^*}}-1} \frac{m^p {}_{SU_{i^*}}}{P!\lambda^p {}_{SU_{i^*}}} exp\left(-\frac{m_{SU_{i^*}}\kappa_1\gamma^{(d)}}{\lambda_{SU_{i^*}}\gamma_0\left(\alpha_{U_{i^*}} - \alpha_{V_{j^*}}\gamma^{(d)}\right)}\right) \times \left[\frac{K_1\gamma^{(d)}}{\gamma_0\left(\alpha_{U_{i^*}} - \alpha_{V_{j^*}}\gamma^{(d)}\right)}\right]^p \quad (31)$$

where $K_1 = \gamma_0 {\sigma^2}_{SU_{i^*}} + 1$ and $\lambda_{SU_{i^*}} = \frac{\widehat{\Omega}_{SU_{i^*}}}{\frac{\theta_{SU_{i^*}}}{d_{SU_{i^*}}}} = \frac{\left(1-\phi_{SU_{i^*}}\right)\Omega_{SU_{i^*}}}{\frac{\theta_{SU_{i^*}}}{d_{SU_{i^*}}}}$

Similarly, by substituting (3) and (4) into (24) and solving, gives

$$P^{SV} = 1 - Pr\left\{\frac{\alpha_{U_{i^*}}\gamma_0\left|\hat{h}_{SV_{j^*}}\right|^2}{\alpha_{V_{j^*}}\gamma_0\left|\hat{h}_{SV_{j^*}}\right|^2|h_{rr}|^2 + \gamma_0{\sigma^2}_{SV_{j^*}} + 1} \geq \gamma^{(d)}, \frac{\alpha_{V_{j^*}}\gamma_0\left|\hat{h}_{SV_{j^*}}\right|^2}{\gamma_0{\sigma^2}_{SV_{j^*}} + 1} \geq \gamma^{(d)}\right\} \quad (32a)$$

$$P^{SV} = F_{\left|\hat{h}_{SV_{j^*}}\right|^2}\left(\frac{\kappa_2\gamma^{(d)}}{\gamma_0\chi_1}\right) \quad (32b)$$

where $\chi_1 = min\left\{\alpha_{V_{j^*}}, \alpha_{U_{i^*}} - \alpha_{V_{j^*}}\gamma^{(d)}\right\}$ and $\kappa_2 = \gamma_0{\sigma^2}_{\mathrm{SV}_{j^*}} + 1$. Thus, the probability P^{SV} is obtained as

$$P^{SV} = 1 - \sum_{p=0}^{mP_{SV_{j^*}}-1} \frac{mp_{SV_{j^*}}}{P!\lambda p_{SV_{j^*}}}\left(\frac{\kappa_2\gamma^{(d)}}{\gamma_0\chi_1}\right)^p exp\left(-\frac{m_{SV_{j^*}}k_2\gamma^{(d)}}{\lambda_{SV_{j^*}}\gamma_0\chi_1}\right) \quad (33)$$

where $\lambda_{SV_{j^*}} = \frac{\widehat{\Omega}_{SV_{j^*}}}{\frac{\theta_{SV_{j^*}}}{d_{SV_{j^*}}}} = \frac{\left(1-\phi_{SV_{j^*}}\right)\Omega_{SV_{j^*}}}{\frac{\theta_{SV_{j^*}}}{d_{SV_{j^*}}}}$

Also, by substituting (19) and (20) into (25), gives

$$P^{SR_kUV} = Pr\left\{\max_{1\leq k\leq K}\left\{min\left\{\begin{matrix}\gamma_{SR_k}^{x_{U_{i^*}}}, \gamma_{SR_k}^{x_{V_{j^*}}}, \gamma_{R_kU_{i_*}}^{x_{U_{i^*}}}, \\ \gamma_{R_kV_{j^*}}^{x_{U_{i^*}}}, \gamma_{R_kV_{j^*}}^{x_{V_{j^*}}}\end{matrix}\right\}\right\} < \varepsilon^{(d)}\right\} \quad (34)$$

According to [5], Equation (34) can be approximated as

$$P^{SR_kUV} = \prod_{k=1}^{K}\left\{1 - Pr\left\{\begin{matrix}\gamma_{SR_k}^{x_{U_{i^*}}} \geq \varepsilon^{(d)}, \gamma_{SR_k}^{x_{V_{j^*}}} \geq \varepsilon^{(d)}, \\ \gamma_{R_kU_{i^*}}^{x_{U_{i^*}}} \geq \varepsilon^{(d)}, \gamma_{R_kU_{i^*}}^{x_{U_{i^*}}} \geq \varepsilon^{(d)}, \\ \gamma_{R_kV_{j^*}}^{x_{V_{j^*}}} \geq \varepsilon^{(d)}\end{matrix}\right\}\right\}. \quad (35)$$

After algebraic simplification and by utilizing the fundamental properties of probabilities, the probability P^{SR_kUV} can be expressed as

$$P^{SR_kUV} = \prod_{k=1}^{K}\left(1-\left[1-F_{\left|\hat{h}_{R_kU_{i^*}}\right|^2}\left\{\frac{\gamma_{R_k}\sigma^2{}_{R_kU_{i^*}}\varepsilon^{(d)}+\varepsilon^{(d)}}{\left(\beta_{U_{i^*}}-\beta_{V_{j^*}}\varepsilon^{(d)}\right)\gamma_{R_k}}\right\}\right]\times\left[1-F_{\left|\hat{h}_{R_kV_{j^*}}\right|^2}\left\{\frac{\varepsilon^{(d)}\gamma_{R_k}\sigma^2{}_{R_kV_{j^*}}+\varepsilon^{(d)}}{\chi_3\gamma_{R_k}}\right\}\right]\right) \quad (36)$$

where $\chi_2 = \beta_{U_{i^*}} - \beta_{V_{j^*}}\gamma^{(d)}, \chi_3 = min\left\{\beta_{V_{j^*}}, \chi_2\right\}$

Using the CDF of the channel $\left|\hat{h}_{R_kU_{i^*}}\right|^2$ and $\left|\hat{h}_{R_kV_{j^*}}\right|^2$, the closed-form expression for the probability is derived as

$$P^{SR_kUV} = \prod_{k=1}^{K}\left(1-\left(1-\sum_{p=0}^{m_{R_kU_{i^*}}-1}\sum_{q=0}^{m_{R_kV_{j^*}}-1}\frac{m^p{}_{R_kU_{i^*}}}{P!\lambda^p{}_{R_kU_{i^*}}}\Xi_1\times\frac{m^q{}_{R_kV_{j^*}}}{P!\lambda^p{}_{R_kV_{j^*}}}\Xi_2\right)\right) \quad (37)$$

where $\Xi_1 = \left[\frac{\gamma_{R_k}\sigma^2{}_{R_kU_{i^*}}\gamma^{(d)}+\gamma^{(d)}}{\left(\beta_{U_{i^*}}-\beta_{V_{j^*}}\gamma^{(d)}\right)\gamma_{R_k}}\right]^p exp\left(-\frac{m_{R_kV_{j^*}}\left(\gamma^{(d)}\gamma_{R_k}\sigma^2{}_{R_kV_{j^*}}+\gamma^{(d)}\right)}{\lambda_{R_kV_{j^*}}\chi_3\gamma_{R_k}}\right)$,

$\Xi_2 = \left[\frac{\varepsilon^{(d)}\gamma_{R_k}\sigma^2{}_{R_kV_{j^*}}+\varepsilon^{(d)}}{\chi_3\gamma_{R_k}}\right]^q exp\left(-\frac{m_{R_kV_{j^*}}\left(\varepsilon^{(d)}\gamma_{R_k}\sigma^2{}_{R_kV_{j^*}}+\varepsilon^{(d)}\right)}{\lambda_{R_kV_{j^*}}\chi_3\gamma_{R_k}}\right)$,

$\lambda_{R_kU_{i^*}} = \frac{\widehat{\Omega}_{R_kU_{i^*}}}{\bar{L}_{R_kU_{i^*}}} = \frac{\left(1-\phi_{R_kU_{i^*}}\right)\Omega_{R_kU_{i^*}}}{\bar{L}_{R_kU_{i^*}}}$, and $\lambda_{R_kV_{j^*}} = \frac{\widehat{\Omega}_{R_kV_{j^*}}}{\bar{L}_{R_kV_{j^*}}} = \frac{\left(1-\phi_{R_kV_{j^*}}\right)\Omega_{R_kV_{j^*}}}{\bar{L}_{R_kV_{j^*}}}$.

2.3 Outage Probability Problem Formulation

The optimization problem lies in determining not only the UAVR altitude but also the harvested energy ratios (τ and ρ), power allocation and fraction of received power at the UAVR to ensure that the outage probability is minimized. Thus, the objective function which is to minimize the outage probability performance is obtained by substituting equations (31), (33) and (37) into (22) constrained to system parameters is represented in equation (38) as

$$\begin{aligned}\min_{\rho,\tau,\alpha_{U_i},\alpha_{V_j},\beta_{U_i},\beta_{V_j}} \quad & P_{out} = P^{SR_kUV}\left(P^{SU}+P^{SV}-P^{SU}P^{SV}\right)\\ s.t. \quad & C1: 0 \le \rho \le 1\\ & C2: 0 \le \tau \le 1\\ & C3: \alpha_{U_i}+\alpha_{V_j} = 1\\ & C4: \beta_{U_i}+\beta_{V_j} = 1\end{aligned} \quad (38)$$

Constraints C1 and C2 are to ensure optimal energy harvesting ratios ($\rho, \tau \in \{0,1\}$) to obtain the minimal outage probability for reliable communication between the source and destinations. Constraints C3 ensure that the source optimally allocate power coefficient and C4 are used to obtain the optimal NOMA power allocations add up to the total available transmit power, both at the source and at the UAVR.

2.4 Solution to the Formulated Problem using Enhanced Duck Swarm Algorithm

The formulated optimization problem of the proposed full-duplex HTPS scheme for UAV-aided CNOMA systems was solved using EDSA. The EDSA is a modification of the conventional DSA with RWS which uses probabilistic selection to balance exploration and exploitation, preserving diversity by allowing weaker solutions a chance of selection. This prevents repeated selection of the same leader and reduces the risk of entrapment in local minima rather than deterministic approach by the greedy selection in the conventional DSA. In this paper, each duck represents a candidate solution, while the leader duck corresponds to the best solution at each iteration. The swarm updates its positions by learning from both the leader and neighboring ducks, enabling broad exploration of the search space and reducing the risk of local optima. The EDSA operates in two coordinated phases: an exploration phase, where ducks spread across the solution space using stochastic movements, and an exploitation phase, where the search is refined around the leader for precise convergence. Adaptive parameters such as the control parameter of global search (μ), the searching conversion probability of exploration phase (P), KF_1 and KF_2 which denote the cooperation and competition coefficient between ducks in the exploitation phase, respectively, and other control coefficients regulate the balance between these phases.

Through continuous position updates, fitness evaluations, and leader selection, the swarm gradually converges toward the global optimum while maintaining boundary feasibility. As reflected in Algorithm 1, the method enhances the optimization of time-switching and power splitting ratios, strengthens resource allocation, reduces outage performance and user fairness. Thus, EDSA possesses a computational complexity of $O\left(T_{\max}\left(NC_f + N\,log\,N\right)\right)$ with the total runtime dominated by evaluating the fitness of N candidate solutions across $T_{\max}$ generations, C_f is the objective function cost and a small additional $N\,log\,N$ cost per generation for ranking making DSA enhanced with RWS computationally complex comparable to the conventional DSA in UAV-aided full duplex, decode and forward cooperative NOMA network.

Algorithm 1: HTPS-EDSA based UAV-aided CNOMA network

1) Begin
2) Input Initialization parameters: population size $\boldsymbol{N}$, maximum iterations $\boldsymbol{T_{max}}$, constant multiplier $\boldsymbol{K}$
   define search space bounds $\boldsymbol{\rho} \in [\mathbf{0},\mathbf{1}]$, $\boldsymbol{\tau} \in [\mathbf{0},\mathbf{1}]$, $\boldsymbol{\alpha_{U_i}}, \boldsymbol{\alpha_{V_j}} \in [\mathbf{0},\mathbf{1}]$ with $\boldsymbol{\alpha_{U_i}} + \boldsymbol{\alpha_{V_j}} = \mathbf{1}$, $\boldsymbol{\beta_{U_i}}, \boldsymbol{\beta_{V_j}} \in [\mathbf{0},\mathbf{1}]$ with $\boldsymbol{\beta_{U_i}} + \boldsymbol{\beta_{V_j}} = \mathbf{1}$
3) Randomly initialize duck swarm positions $\boldsymbol{X_i} = \left[\boldsymbol{\rho_i}, \boldsymbol{\tau_i}, \boldsymbol{\alpha_{U_i}}, \boldsymbol{\alpha_{V_j}}, \boldsymbol{\beta_{U_i}}, \boldsymbol{\beta_{V_j}}\right], \boldsymbol{i} = \mathbf{1}, \mathbf{2}, \ldots, \boldsymbol{N}$
4) Define objective function $\boldsymbol{f(X_i)} = \boldsymbol{P}_{\text{out}} = \boldsymbol{P}^{\text{SR}_k\text{UV}}(\boldsymbol{P}^{\text{SU}} + \boldsymbol{P}^{\text{SV}} - \boldsymbol{P}^{\text{SU}}\boldsymbol{P}^{\text{SV}})$
5) Calculate fitness $\boldsymbol{f(X_i)}$ for each duck in the swarm, Identify the best fitness value $\boldsymbol{f_{\min}} = \mathbf{min}\,(\boldsymbol{f(X_i)})$ and select the leader position $\boldsymbol{X}_{\text{leader}}$ corresponding to $\boldsymbol{f_{\min}}$
6) While t < $\boldsymbol{T_{max}}$ do *% Start Iteration Loop*
7) Update $\boldsymbol{\mu} = \boldsymbol{K} \cdot \left(\mathbf{1} - \frac{\boldsymbol{t}}{\boldsymbol{T_{\max}}}\right)$ and $\boldsymbol{P}$, $\boldsymbol{KF_1}$ *and* $\boldsymbol{KF_2}$
8) For i = 1 to N: *%Exploration Phase*
9) Compute fitness-based probabilities for each duck $\boldsymbol{p_i} = \frac{\boldsymbol{f(X_i^t)}}{\sum_{j=1}^{N} \boldsymbol{f(X_j^t)}}$ *(for minimization problems)* or $\boldsymbol{p_i} = \frac{\mathbf{1}/\boldsymbol{f(X_i^t)}}{\sum_{j=1}^{N} \mathbf{1}/\boldsymbol{f(X_j^t)}}$ *using rank-based probabilities and c*alculate cumulative probabilities: $\boldsymbol{C_i} = \sum_{\boldsymbol{j=1}}^{\boldsymbol{i}} \boldsymbol{p_j}$
10) Generate random number $\boldsymbol{r_1} \in [\mathbf{0},\mathbf{1}]$ and $\boldsymbol{r_2} \in [\mathbf{0},\mathbf{1}]$ then select parents $\boldsymbol{X_a}$ and $\boldsymbol{X_b}$, respectively where $\boldsymbol{C_{a-1}} < \boldsymbol{r_1} \leq \boldsymbol{C_a}$ and $\boldsymbol{C_{b-1}} < \boldsymbol{r_2} \leq \boldsymbol{C_b}$ accordingly *%Select Two Parent Positions*
11) *Update position* $\boldsymbol{X_i^{t+1}} = \boldsymbol{X_i^t} + \boldsymbol{\mu} \cdot \boldsymbol{X_i^t} \cdot \text{sign}(\boldsymbol{r} - \mathbf{0.5})$ If $\boldsymbol{P} >$ rand *%(Exploration) using Selected Parents*
    $\boldsymbol{X_i^{t+1}} = \boldsymbol{X_i^t} + \boldsymbol{CF_1} \cdot (\boldsymbol{X_{\text{leader}}^t} - \boldsymbol{X_i^t}) + \boldsymbol{CF_1} \cdot (\boldsymbol{X_j^t} - \boldsymbol{X_i^t})$ if otherwise *or*
    $\boldsymbol{X_i^{t+1}} = \boldsymbol{X_i^t} + \boldsymbol{C_1} \cdot \boldsymbol{\mu} \cdot (\boldsymbol{X_i^t} - \boldsymbol{C_1} \cdot \boldsymbol{X_{\text{leader}}^t}) \cdot \text{sign}(\boldsymbol{r} - \mathbf{0.5}) + \boldsymbol{CF_1} \cdot (\boldsymbol{X_{\text{leader}}^t} - \boldsymbol{X_i^t}) + \boldsymbol{CF_1} \cdot (\boldsymbol{X_j^t} - \boldsymbol{X_i^t})$
12) Clip $\boldsymbol{\rho}, \boldsymbol{\tau}$ to $[\mathbf{0}, \mathbf{1}]$ *%Ensure all variables remain within their feasible ranges*
    Enforce $\boldsymbol{\alpha_{u_i}} + \boldsymbol{\alpha_{v_j}} = \mathbf{1}$ by normalizing $\boldsymbol{\alpha_{u_i}} = \frac{\boldsymbol{\alpha_{u_i}}}{\boldsymbol{\alpha_{u_i}} + \boldsymbol{\alpha_{v_j}}}, \boldsymbol{\alpha_{v_j}} = \frac{\boldsymbol{\alpha_{v_j}}}{\boldsymbol{\alpha_{u_i}} + \boldsymbol{\alpha_{v_j}}}$ and $\boldsymbol{\beta_{u_i}} + \boldsymbol{\beta_{v_j}} = \mathbf{1}$
13) Calculate new fitness $\boldsymbol{f}_{\text{new}} = \boldsymbol{f(X_i^{t+1})}$
14) Collect all improved positions and their fitness values *%update leader using Roulette Wheel Selection*
15) Compute selection probabilities for candidate leaders using $\boldsymbol{p}_{\text{leader},\boldsymbol{k}} = \frac{\mathbf{1}/\boldsymbol{f(X_k)}}{\sum_{j=1}^{N} \mathbf{1}/\boldsymbol{f(X_j)}}$
16) Generate random number $\boldsymbol{r} \in [\mathbf{0},\mathbf{1}]$ and select new leader based on roulette wheel
17) $\boldsymbol{X}_{\text{leader}} = \boldsymbol{X_k}$ where $\boldsymbol{C_{k-1}} < \boldsymbol{r} \leq \boldsymbol{C_k}$

---

18) If $f_{\text{new}} < f_{\min}$, *%update using Roulette Wheel Selection*
19) $X_{\text{leader}} = X_i^{t+1}, f_{\min} = f_{\text{new}}$
20) End if
21) End For
22) For i = 1 to N: *%Exploitation Phase*
23) Calculate selection probabilities for all ducks using fitness values using $p_i = \frac{1/f(X_i^t)}{\sum_{j=1}^{N} 1/f(X_j^t)}$ *%for minimization:*
24) Apply roulette wheel and select two random individuals X_k and X_j
25) If $f(X_i^t) > f(X_i^{t+1})$ *%update position*
26) $X_i^{t+1} = X_i^t + \mu \cdot (X_{\text{leader}}^t - X_i^t)$
27) Else
28) $X_i^{t+1} = X_i^t + KF_1 \cdot (X_{\text{leader}}^t - X_i^t) + KF_1 \cdot (X_k^t - X_j^t)$
29) Apply condition in step 12
30) end if
31) Calculate new fitness $f_{\text{new}} = f(X_i^{t+1})$
32) If $f_{\text{new}} < f(X_i^t)$
33) X_i^{t+1} replaces position X_i^t *and* f_{new} replaces fitness $f(X_i^t)$
34) End if
35) Create a pool of candidate solutions (all individuals with improved fitness)
36) Compute selection probabilities $p_{\text{leader},k} = \frac{1/f(X_k)}{\sum_{j=1}^{M} 1/f(X_j)}$, where M is the number of candidate solutions
37) Apply cumulative probability distribution
38) Select new leader using roulette wheel $X_{\text{leader}} = X_k$ where $C_{k-1} < r \leq C_k$
39) Update $f_{\min} = f(X_{\text{leader}})$
40) End For
41) $t = t + 1$
42) End While
43) Output $X_{best} = [\rho^*, \tau^*, \alpha_{u_i}^*, \alpha_{v_j}^*, \beta_{u_i}^*, \beta_{v_j}^*]$, $f_{min} = P_{out}^*$
44) End

3. RESULTS AND DISCUSSION

This section presents the effect of varying system parameters on outage probability performance of the network with coordinate $S\ (0,0,0);\ R_k(1,1,h_R);\ U_i(2,3,0)$ and $U_i(4,5,0)$. The Monte Carlo simulation was conducted in the MATLAB R2023a environment using random seed values ran over 10^4 runs with the simulation parameters presented in Table 2. Also, the comparison of the HTPS-EDSA scheme with other existing schemes such as the conventional HTPS, HTPS-BAO and HTPS-DSA was performed.

Table 2: Simulation parameters

Parameters	**Value**
Transmit power	-10 dB to 10 dB
UAV altitude	0 to 20 m
Coordinates	S (0,0,0); R (1,1,h_R); U_i (2,3.0); V_j (4,5,0)
Channel	Nakagami-m
Rate	0.1 bps
Noise power	0.01, 0.02, 0.03
Number of users	4
Pathloss exponent	3
Energy conversion coefficient	0.8

Fig. 3 depicts the outage probability of the proposed HTPS-EDSA scheme for different values of antenna k was plotted against transmitting power at optimal values of energy harvesting time, power splitting and power allocation at noise variance $\sigma^2 = 0.01$, UAVR altitude $h_R = 20\,m$. It is observed that the outage probability of HTPS-EDSA scheme decreases as the transmit power γ_0 increases from –10 dB to 10 dB. For $k = 2$, the outage probability decreased significantly from 0.5 at –10 dB to 3.6175 $\times 10^{-5}$ at 10 dB, for value of $k = 3$, the outage probability was 9.0167 $\times 10^{-2}$ and 3.5146 $\times 10^{-8}$ at -10 dB and 10 dB respectively. Also, for value of $k = 4$, outage probability reduced from 2.5501$\times$ 10^{-2} to 1.275 $\times 10^{-9}$. This shows that increasing the antenna diversity results in consistently reduction in outage probability across all transmit power levels. The proposed HTPS-EDSA scheme which agreed in both the analytical and through Monte Carlo simulation showed superiority with an outage probability value of 1.275 $\times$ 10^{-9} against the conventional HTPS, HTPS-BAO and HTPS-DSA which gave 7.075 $\times$ 10^{-6}, 1.657 $\times$ 10^{-8} and 2.325 $\times$ 10^{-9}, respectively at transmitting power of 10 dB and k value of 4. This indicates that the employing HTPS-EDSA scheme in UAV-aided cooperative NOMA system in full duplex mode with optimal resource allocation demonstrates the capability of achieving better outage performance at both the near and far users.

Fig. 4 depicts the outage probability against varying UAVR altitude for different values of antenna at optimal values of energy harvesting time, power splitting and power allocation, noise variance $\sigma^2 = 0.01$ and transmitting power of 10 dB. The results revealed a substantial reduction in outage probability performance as the UAVR altitude increases for all the schemes. It was observed that at altitudes beyond 14 m, saturation regions were attained for most of the schemes. This was because at this altitude, there were no significant changes in the outage probability performance. In the figure, at $k = 2$ the outage probability declines from 0.7 at ground level to 2.234$\times$ 10^{-3} at 10 m and saturates to 1.324$\times$ 10^{-3} beyond 16 m. Also, for $k = 3$, the outage probability was 0.4, 2.2748$\times$ 10^{-5} and 1.26$\times$ 10^{-5} at ground, altitude of 10 m and 14 m, respectively. Moreso, for $k = 4$ the values of outage probability obtained at ground level was 0.34 and further decreased to 5.137$\times$ 10^{-7} at 10 m and saturates to 2.788$\times$ 10^{-7} at 14 m. This suggests that higher value of antenna k yields superior diversity gains and system resilience due to dominance LoS between the source, UAVR and users. Comparing the outage probability performance of the schemes at saturation showed that the proposed HTPS-EDSA recorded a value of 2.905$\times$ 10^{-7} against conventional HTPS, HTPS-BAO and HTPS-DSA schemes with 3.055$\times$ 10^{-3}, 6.875$\times$ 10^{-6} and 5.115$\times$ 10^{-7}, respectively. The proposed HTPS-EDSA scheme employed in UAV-aided CNOMA system established a reliable LoS communication links between ground users and the UAV at an optimal altitude of 14 m notably to mitigate the impact of multipath fading and shadowing.

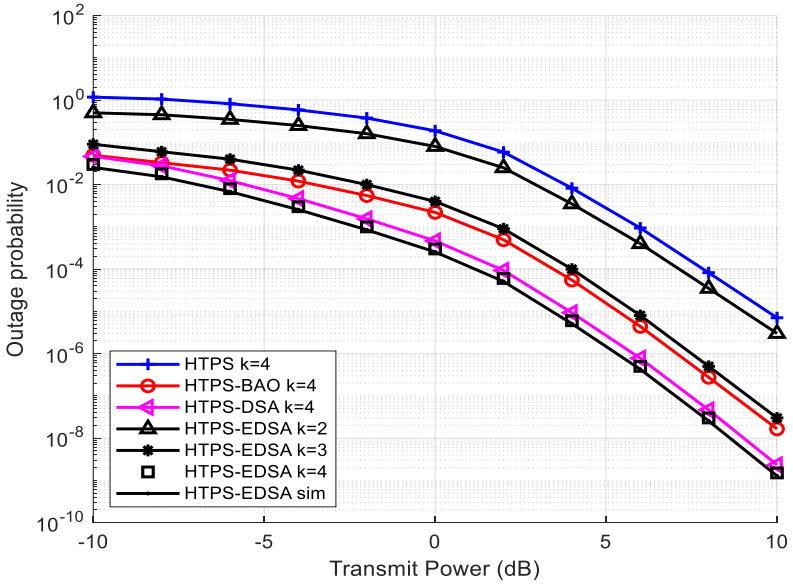


Fig. 3: Outage probability against transmitting power for different antennas values.

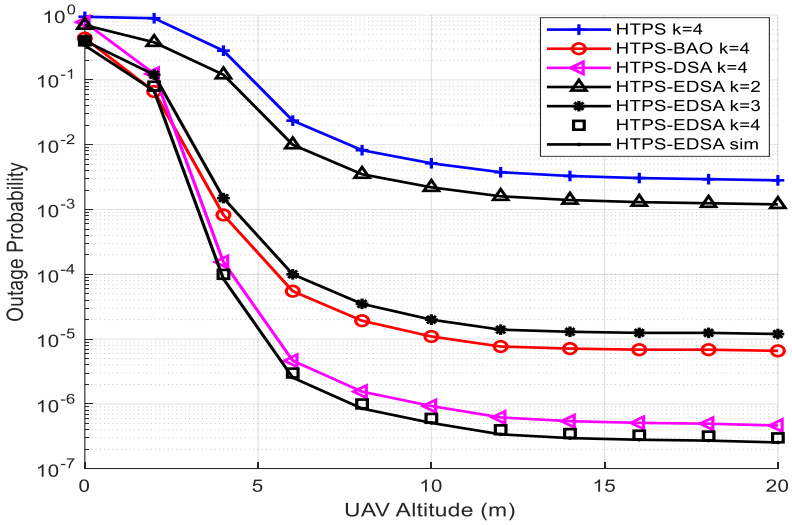


Fig. 4: Outage probability against UAV altitude for different antennas values.

The impact of the power splitting ratio ρ on the outage probability is depicted in Fig. 5 at the antenna value $k = 3$ at optimal values of energy harvesting time, power allocation and transmitting power of 10 dB. The outage probability initially decreases with increasing ρ until it reaches an optimal point and then degrades as ρ approaches higher values which is evident in all values of the noise variance. Observation from Fig. 5 shows that for the proposed HTPS-EDSA scheme at $\sigma^2 = 0.03$, gave an outage probability decreases significantly to 3.2651×10^{-7}, 1.551×10^{-7} at $\sigma^2 = 0.02$ and 5.071×10^{-8} at $\sigma^2 = 0.01$ all obtained at optimal value of $\rho = 0.7$. This represents a balanced allocation between energy harvesting and information decoding with less effect of noise variance at the lowest value. The outage probability obtained at $\sigma^2 = 0.01$ for the proposed HTPS-EDSA, conventional HTPS, HTPS-BAO and HTPS-DSA schemes were 5.271×10^{-8}, 3.527×10^{7}, 1.12×10^{-8} and 7.65×10^{-8}, respectively. This indicates that a better system outage probability performance can be guaranteed at lower value of noise variance while transmitting via the UAVR at optimal system resource allocation.

Fig. 6 shows the graph of outage probability against energy harvesting time τ at different user diversity configuration $i = j$ with $k = 3$, $\sigma^2 = 0.01$ at optimal values of fraction of received power, power allocation and transmitting power of 10 dB. The results show that the outage probability values decreased progressively with increasing fraction of energy harvesting time τ with clear distinctions across the different levels of user configurations. In the proposed HTPS-EDSA scheme for user's configuration of $i = j = 2$, the outage probability reduces from 2.85×10^{-5} at $\tau = 0.1$ to 2.45×10^{-8} at $\tau = 0.9$. Also, for $i = j = 3$, at $\tau = 0.1$ and 0.9, the outage probability values were 1.057×10^{-5} and 2.5970×10^{-9}, respectively, while the corresponding values for $i = j = 4$ were 2.4501×10^{-6} and 2.125×10^{-10}. It can be observed that at the user configuration increased, the outage probability performance becomes much better. The proposed HTPS-EDSA scheme with outage probability performance of 9.125×10^{-8} which outperformed the conventional HTPS, HTPS-BAO and HTPS-DSA schemes with 3.527×10^{-7}, 3.75×10^{-7} and 1.395×10^{-10}, respectively, at optimal $\tau = 0.5$. This demonstrated an increase in user diversity order substantially improving the system robustness.

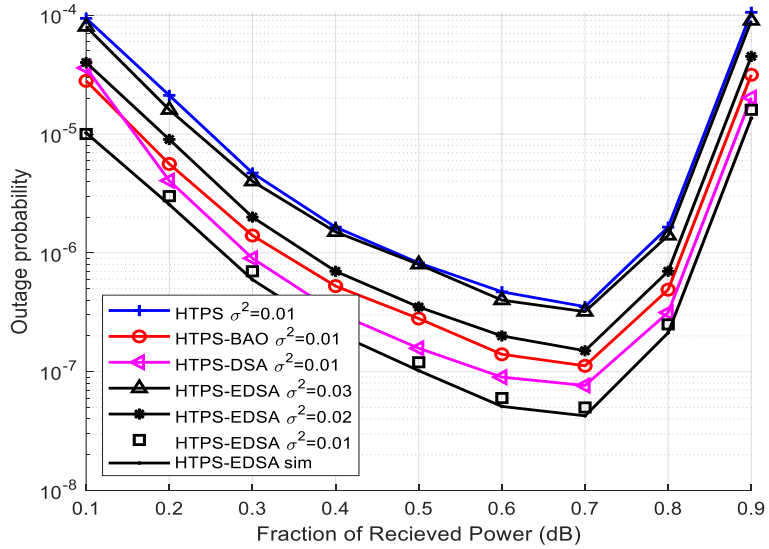


Fig. 5: Outage probability against fraction of received power ρ for different noise variance.

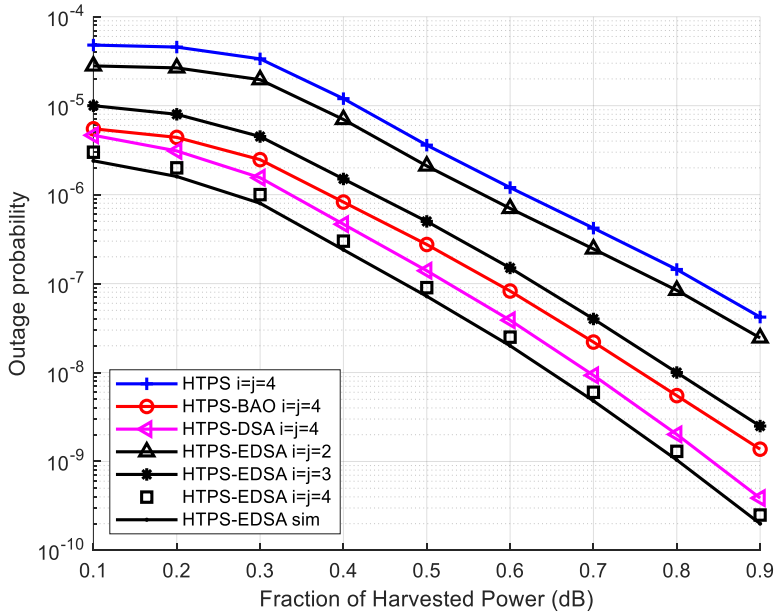


Fig. 6: Outage probability against fraction of energy harvesting time τ at different user diversity configuration.

The plot in Fig. 7 highlights the convergence speed and accuracy of the proposed scheme. The proposed HTPS-EDSA scheme achieved the fastest convergence and lowest fitness value of 0.0155, compared to HTPS-DSA with 0.020, while HTPS-BAO with the slowest and least accurate with 0.023. The EDSA with RWS-based leader update demonstrated a clear convergence benefit of approximately 22% better than DSA and 33% better than BAO. This improvement emanated from its ability to balance global and local search, preserve population diversity and avoid premature convergence to local optima. These results confirm the validity of the proposed enhancement to DSA with RWS as an effective optimization algorithm for UAV-aided CNOMA.

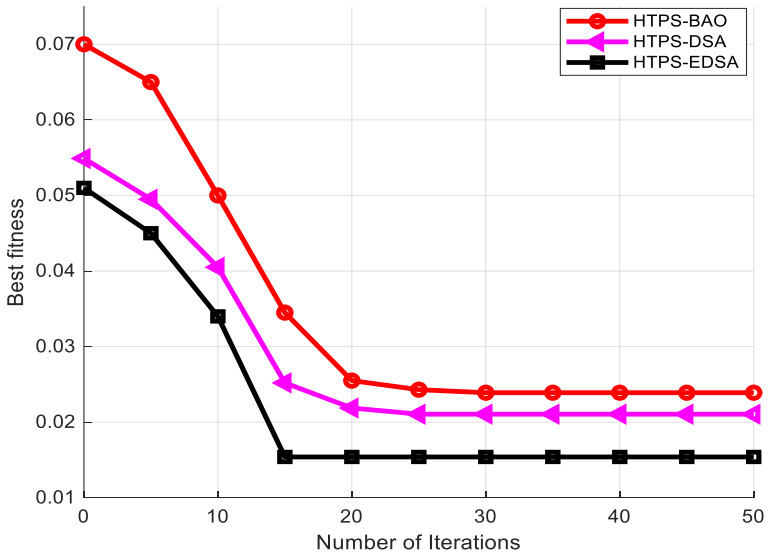


Fig. 7: Best fitness against iteration.

The average fitness plot in Fig. 8 demonstrates the superiority of HTPS-EDSA to the conventional HTPS-DSA and HTPS-BAO algorithms. For all three algorithms, the average fitness decreases as the number of iterations increases. The effectiveness of the exploration–exploitation trade-off in HTPS-EDSA is evident in the steepest early descent from 0.270 to 0.070 in 10 iterations attained a faster and stable convergence of 0.032 at 15 iterations. This suggests that there is a clear transition from broad exploration to focused exploitation. The proposed HTPS-EDSA, enhanced with RWS, maintains a fitness margin of 0.0195 between the average and best values, suggesting that the population maintains diversity at convergence rather than collapsing prematurely. This results in an improvement of 5.71% and 28.6% over conventional HTPS-DSA and HTPS-BAO, respectively. This gain is achieved due to the RWS mechanism, which selects parents based on a fitness-dependent probabilistic basis rather than randomly or greedily. Thus, HTPS-EDSA is the most efficient algorithm for optimizing UAV-based CNOMA design parameters.

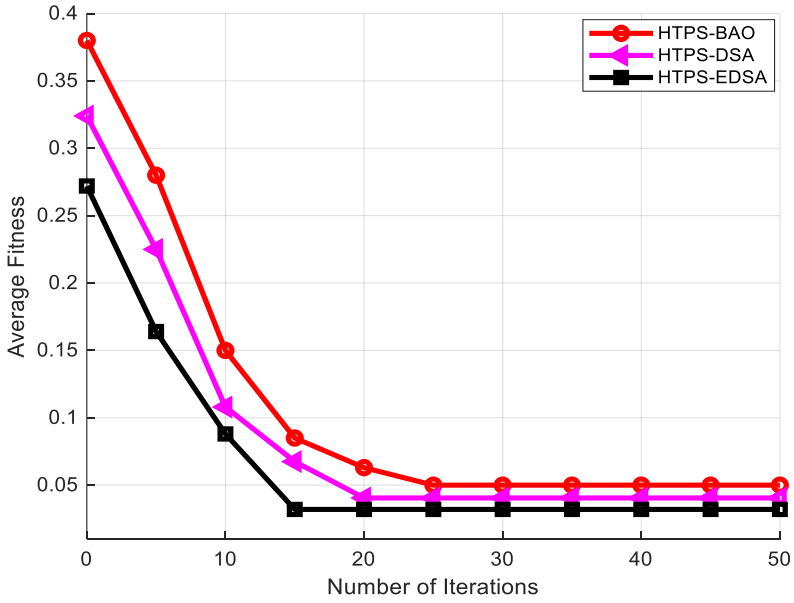


Fig. 8: Average fitness against iteration.

4. CONCLUSION

This paper focused on minimizing the outage performance of FD UAV-aided CNOMA network using HTPS scheme. The closed-form outage-probability expression was derived for the network over Nakagami-m fading channels. An outage probability optimization problem was formulated. The formulated problem was solved using DSA enhanced with RWS mechanism. The proposed HTPS-EDSA scheme was simulated in MATLAB

software environment using the network system parameters. The outage probability performance was evaluated and compared with conventional HTPS, HTPS-DSA and HTPS-BOA. The results showed that outage probability performance of the proposed HTPS-EDSA scheme is superior to that of other schemes at optimal system parameter. The proposed protocol is suitable for UAV-aided CNOMA networks for improved and reliable communication. The future works can investigate the impact of applying non-linear hybrid SWIPT models on the UAV-aided cooperative network.

REFERENCES

[1] Ji, B., Li, Y., Zhou, B., Li, C., Song, K., and Wen, H. "Performance analysis of UAV relay assisted IoT communication network enhanced with energy harvesting". *IEEE Access, vol.* 7, 2019, pp. 38738-38747.

[2] Akande D. O. and Salleh M. F. M. "A Multi objective target-oriented cooperative MAC protocol for wireless ad-hoc networks with energy harvesting". *IEEE Access*, vol. 8, 2020, pp. 25310-25324.

[3] Zhou, X., Zhang, R. and Ho, C. K. "Wireless information and power transfer: Architecture design and rate-energy tradeoff". *IEEE Transactions on Communications,* vol. 61, no. 11, pp. 4754–4767.

[4] Ojo, F. K., Akande, D. O., and Salleh, M. F. M. "An overview of RF energy harvesting and information transmission in cooperative communication networks". *Telecommunication Systems*, 70, no. 2, 2019, pp. 295–308.

[5] Vo, V. N., Dang, V. H., Tran, H., Tran, D. D., Chatzinotas, S., Quoc, H. L., So-In, C., Truong, V. T., and Ho, T. D. "Performance optimization for hybrid TS/PS SWIPT UAV in cooperative NOMA IoT networks". *Alexandria Engineering Journal*, vol. 107, 2024, pp. 559–567.

[6] Akande D. O., Ojo F.K., Ojo S.I., and Oseni O. F. "Adaptive cooperative MAC with energy harvesting for multi-objective performance in wireless ad-hoc networks", *Nigerian Journal of Technological Development*, vol. 22, no. 4, 2025, pp. 113-123.

[7] Hu, X., Wen, P., Xiao, H., Wang, W., and Wong, K. K. "Maximizing energy charging for UAV-assisted MEC systems with SWIPT". *arXiv preprint arXiv:2403.03756*, 2024

[8] Akande, D. O., Oseni, O. F., Ojo, F. K., Adeleke, J. A. and Fawole, A. O. "Outage probability performance of hybrid time-power splitting relaying protocol with interferers presence". *ABUAD Journal of Engineering Research and Development*, vol. 8, no. 1, 2025, pp. 324-332.

[9] Ding, Z., Schober, R., and Poor, H. V. "A general MIMO framework for NOMA downlink and uplink transmission based on signal alignment". *IEEE Transactions on Wireless Communications*, vol. 18, no. 12, 2017 pp. 6386–6402.

[10] Islam, S. M. R., Zeng, M., Dobre, O. A. and Kwak, K. "Non-orthogonal multiple access (NOMA): How It meets 5G and beyond". *arXiv preprint*, arXiv:1907.10001, 2019.

[11] Ding, Z., Dai, H. and Poor, H. V. (2016), Relay selection for cooperative NOMA." *IEEE Wireless Communications Letters*, vol. 5, no. 4, 2016, pp. 416–419.

[12] Liu, H., Ding, Z., Kim, K. J., Kwak, K., and Poor, H. V. "Decode-and-forward relaying for cooperative NOMA systems with direct links". *IEEE Transactions on Wireless Communications*, vol. 17, no. 12, 2018, pp. 8077–8093.

[13] Zeng Z. M., Hao H., Dobre O. A., Ding Z., and Poor H. V. Power minimization for multi-cell uplink NOMA with imperfect SIC*". IEEE Wireless Communications Letters*, vol.8, no. 12, 2020, pp. 2030-2024.

[14] Mu, G. "Joint beamforming and power allocation for wireless powered UAV-assisted cooperative NOMA systems". *EURASIP Journal on Wireless Communications and Networking*, vol. 2020, no. 55, 2020, pp. 1-14.

[15] Liu, X., Wang, J., Zhao, N., Chen, Y., Zhang, S., Ding, Z., and Yu, F. R. "Placement and power allocation for NOMA-UAV networks". *IEEE Wireless Communications Letters*, vol. 8, no. 3, 2019, pp. 965-968.

[16] Al-Imari M., Xiao P., Imran M. A., and Tafazolli R. "Uplink non-orthogonal multiple access for 5G wireless networks". in *Proc. 11th Int. Symp. Wireless Commun. Syst.*, 2014, pp. 781–785.

[17] Zeng, Y., Zhang, R., and Lim, T. J. "Wireless communications with unmanned aerial vehicles: opportunities and challenges". *IEEE Communications Magazine*, vol. 54, no. 5, 2016, pp. 36–42,

[18] Alharbi, T. E. A. "Resource allocation and energy harvesting in UAV-assisted full-duplex cooperative NOMA systems". *Mathematics*, vol. 13, no. 21, 2025, pp. 3544,

[19] Sadeeq, A. Y., and Ahmed, M. A. "UAV-BS-based hybrid OMA-NOMA system with multiple antennas for multi-user communication". *Journal of Telecommunications and Information Technology*, vol. 100, no. 2, 2025, pp. 38–45.

[20] Zhang, Y., and Wen, Y. "Duck swarm algorithm: theory, numerical optimization, and applications". *Cluster Computing*, vol. 27, 2024, pp. 6441–6469.

[21] Zhang, J., Ge, J., Ni, Q., Wen, M., and Zhang, Y. (2018) Performance Analysis of User Ordering Schemes in Cooperative Power-Domain Non-Orthogonal Multiple Access Network, *IEEE Access*, 6, 47319–47331,

[22] Nguyen, T. L., and Do, D. T. "Power allocation schemes for wireless powered NOMA systems with imperfect CSI: An application in multiple antenna-based relay". *International Journal of. Communication Systems*. vol. 31, no. 15, 2018, pp. 1–17.